Postprint of: Zima B., Kędra R., Baseline-free debonding detection in reinforced concrete structures by elastic wave propagation, Measurement, Vol. 172 (2021), 108907, DOI: 10.1016/j.measurement.2020.108907

Baseline-free debonding detection in reinforced concrete structures by elastic wave propagation

Beata Zima[1], Rafał Kędra[2]

[1]Department of Structural Mechanics
Faculty of Civil and Environmental Engineering
Gdańsk University of Technology
ul. Narutowicza 11/12, 80-233 Gdańsk, Poland
email: beata.zima@pg.edu.pl

[2]Pekabex SA., Budowlanych 54A, 80-298 Gdańsk, Poland

- Experimental and numerical studies in RC specimens with different debonding damages are carried out.
- The wave-based method was used to detect debonding damage in RC beam.
- The measurement of guided wave velocity can provide information about the quality of the steel-concrete adhesive connection.

Abstract

The article presents the results of the numerical and experimental analysis concerning wave propagation in reinforced concrete (RC) beams with various extent of debonding between the steel rod and concrete cover. The main aim of the paper was to consider the unsolved research gaps, which considerably limit the application of wave-based methods in practice. The propagation of the flexural wave modes excited and registered on the outer surface of the concrete cover in RC beams with various damage sizes were considered. The phenomenon of flexural wave propagation in a damaged beam was described theoretically and the relationship between damage size and wave velocity was proposed. Next, the theoretical predictions were examined experimentally. The research allows to observe the variability of the velocity of a wave propagating in various regions of the monitored specimen. The differences between times of flight allow to determine the localization of the debonded rod. The study indicates that the debonding size can be successfully determined if the velocities of flexural wave modes in the concrete specimen as well as in separated reinforcing rod are known.

Keywords: non-destructive testing; guided wave propagation; debonding; reinforced concrete; adhesive connection, flexural wave

1. Introduction

Ultrasonic waves are widely used in structural diagnostics [1]-[4]. The idea of the use of waves is based on the processing and interpreting the characteristics of waves propagating through the investigated object. In recent years the interest of the nondestructive wave-based method has increased significantly, which resulted in the development of various diagnostic approaches. Particularly, the nondestructive methods of the quality assessment of concrete structures have attracted much attention ([5]-[9]), mainly because of the widespread use of reinforced concrete in the civil engineering field. One of the most common and most dangerous damage of reinforced concrete (RC) structures is debonding, which occurs between reinforcement and the concrete cover. Debonding damage significantly reduces the load capacity and durability of the entire structure. The significant potential of elastic wave-based methods in damage detection ([10],[11]), characterization of the damage mode ([12]-[14]) and pre-failure warning [15] has been demonstrated in many previous papers. Elastic waves seemed to be effective also in kissing-bond detection ([16]-[20]). Ultrasonic guided waves were involved by Beard et al. [21] in the inspection of the bonding connection between steel tendons and the concrete. Na et al. [22] investigated high and low-frequency wave propagation in RC beams with a varying debonding length. Sharma et al. [23], Li et al. [24] and Wu and Chang [25] showed that the signal energy increases with increasing extent of debonding between steel and concrete and proved that the signal amplitude can be used as an indicative parameter in the assessment of the adhesive connection quality. Moreover, Wu and Chang [25] also shown that the average wave velocity increases with debonding damage length. The main reason for the velocity changes caused by debonding occurrence is related to wave mode conversion. In general, wave propagates faster in separated steel rebar than in reinforced concrete specimen. When debonding occurs part of wave energy travels along separated steel waveguide which implies the increase of the average wave velocity. The detailed explanation of velocity changes caused by debonding and comprehensive analysis of mode conversion and diffraction in a multilayered specimen was presented in [30]. The exact relationship between wave velocity and debonding size was derived by Zima and Kędra [31]. They showed that the debonding shape or location does not influence the average wave velocity and the total area of the undamaged adhesive connection can be estimated based on the single signal registered at the end of the RC beam. The knowledge about the total area of undamaged steel-concrete connection allowed for nondestructive wave-based estimation of the load-carrying capacity of the pull-out specimen [32], which could be especially useful in diagnostic of rock bolts or grouted tendons. Most recently, the debonding in a concrete-filled steel tube was detected with the use of waves by Xu et al. [33].

Even though in recent years several methods based on wave propagation dedicated to debonding detection in RC structures have been developed, there are still many unsolved research gaps, which considerably limit their application in practice. An example of the unsolved problem is the realization of wave excitation in a place, which is not always accessible. RC beams or columns are generally jointed

at frame nodes. Their ends are anchored in walls or other down stand beams. Meanwhile, the experimental campaigns described above assumed that wave is excited at the uncovered end of the bar exiting the concrete beam, which resulted in triggering mainly longitudinal modes. The paper [25] presents a solution assuming the use of built-in sensors that were placed on a bar surrounded by the concrete cover. Song et al. [26] used the piezoceramic transducers embedded in the concrete structure at pre-determined spatial locations before casting to detect possible cracks inside the reinforced concrete. Despite the high effectiveness of the proposed approaches, they have some limitations. In real engineering structures, the use of a significant number of such embedded sensors would incur significant costs and their installation would significantly extend the time of the construction process. Therefore, it is necessary to consider other solutions that could be put into practice.

The first solution considered would be exposing a single reinforced concrete bar and placing the sensors on the uncovered part (Figure 1a). The sensors attachment on the bar would demand removal of the concrete coating, but in turn, steel is a good waveguide enabling wave propagation over long distances. The second solution would be the attachment of the sensors on the concrete surface (Figure 1b). This way of excitation does not impose the cover removal, but waves, which propagate in a concrete lose their energy much faster and the monitored distance would be shorter than in the case of the excitation in a steel bar. However, in both cases, waves would be excited perpendicularly, which results in the propagation of flexural wave modes, while their application in debonding detection in RC structures has not been considered in detail, yet. In most of the cases considered in the previous papers, only longitudinal waves were excited. Meanwhile, the use of flexural waves raises many of the hitherto unsolved problems.

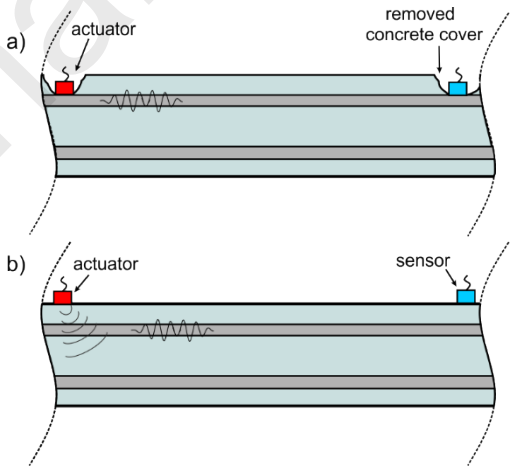

Figure 1 Flexural mode excitation: a) transducers attachment at the uncovered rod and b) transducers attachment on the concrete surface

Moreover, the actual RC structures are usually characterized by the complex reinforcement arrangement and the damage can develop along any reinforcing bar. In the real situation, it is not possible

to predict which bar is debonded to attach the transducers exactly above the damage. Therefore, the practical application requires the analysis of the impact of the mutual debonding-transducers configuration, as well as the influence of additional reinforcement on the wave propagation phenomenon and the output signals.

The article discusses the practical issues related to the application of wave-based methods in debonding detection in RC beams. The paper presents the alternative measurement methodology for using embedded transducers. The main contribution of this paper is the novel baseline-free method of debonded rod localization by using piezo elements attached to the concrete surface. Because the actuation and registration were realized perpendicularly to the beam axis, mainly anti-symmetric modes were triggered. Moreover, the attempt of exact debonding size determining is made and the results are discussed. The detailed analysis of the several aspects, which were not taken into account in the previous studies is presented. The propagation of the flexural wave modes excited and registered on the outer surface of the concrete cover above the bonded and debonded rods was considered. The phenomenon of wave propagation was described and the relationships between the time of flight (ToF) of flexural wave and debonding length were developed. The research allows to observe the variability of the velocity of a wave propagating in various regions of the same, monitored specimen. The relationships differ depending on the placement of the transducers. If the wave propagates along the debonded bar, the formulas describing the relation between ToF of flexural wave and damage size stays in agreement with formulas derived for longitudinal modes excited in steel reinforcement [27]. The decrease of the ToF with debonding size development was observed also in the case of other types of multilayered specimens [28]. However, if the wave was excited above the fully bonded rod, the ToF is described by a nonlinear relationship. The ToF can decrease, increase, or remain the same with debonding size development. The differences between ToFs enable to determine the localization of the debonded reinforcing rod. The study indicates that the debonding size can be accurately determined if the velocities of flexural wave modes in the concrete specimen as well as in separated reinforcing rod are known. The main advantage of the proposed approach is no need to uncover the reinforcement to attach the transducers.

2. Materials and methods

2.1 Geometry of the beam models

The experimental and numerical investigations were carried out on laboratory-scale RC beams of a total length of 50 cm (Figure 2). The cross-section dimensions were 10 cm × 10 cm. The concrete mixture was made of Portland cement type 42 IIIR, sand (0-2 mm) and fine aggregates (2-8 mm). Each beam was reinforced with four smooth steel bars with a diameter of 1 cm. The damage in the form of debonding was artificially introduced by wrapping the reinforcing bar with the cellophane film with very small thickness (90 μm) before casting into concrete. This type of damage is called kissing bond: the concrete cover thoroughly covered the steel rebar, but there was no adhesive connection between layers. In general, bars morphology influences the resistance of steel-concrete adhesive connection, but in this case, it does not influence the results of the nondestructive wave-based testing [29]. Using smooth bars allowed for tight wrapping into cellophane film, which in turn prevented the entry of the cement slurry under its surface.

The debonding damage was located along only one bar and was characterized by varying lengths (0, 20, 30, 40 and 47.6 cm). The material parameters of the concrete and steel were determined during compressive and tensile extensometric tests and were adopted in the further numerical simulations. The averaged values of the material parameters are summarized in Table 1.

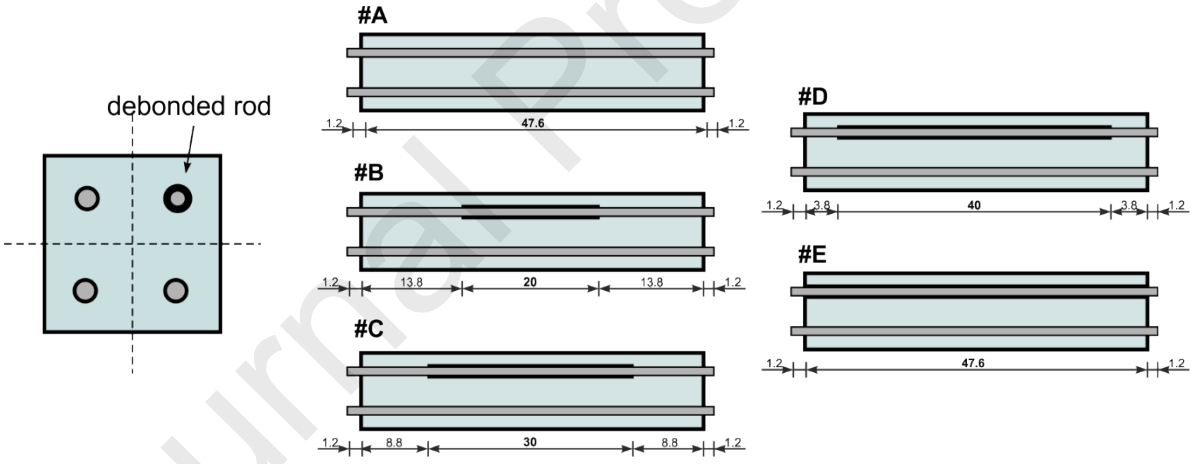

Figure 2 Reinforced concrete beam with partial debonding with extent of a) 0 cm, b) 20 cm, c) 30 cm, d) 40 cm, and e) 47.6 cm

Table 1 Material parameters of steel and concrete

	elastic modulus [GPa]	Poisson's ratio [-]	mass density [kg/m3]
steel	207	0.3	7894
concrete	31.6	0.2	2360

2.2 Numerical models

Numerical simulations of guided wave propagation in RC specimens were performed using the commercial program Abaqus/Explicit based on the finite element method. Eight-nodes brick finite elements with reduced integration (C3D8R) were used to develop numerical models. The mesh convergence study has been performed to establish the appropriate element size. The dimensions of every element did not exceed 2 mm × 2 mm × 2 mm. The element size, as well as the length of the integration step (Δt=1·10-7 s), were assumed on wavelength and wave velocity criteria. The level of discretization was determined by the condition, which says that per the shortest wavelength of interest at least 20 nodes must be introduced in a model. The length of time increment must satisfy the stability condition but also there are some recommendations related to the wave period. An efficient manner is to use at least 20 points per cycle at the highest frequency [34]:

$$\Delta t = \frac{1}{20 f_{\max}} \tag{2}$$

For simplicity, wave excitation by piezo transducer was modeled by the time-dependent concentrated force applied in a chosen node. This approach is justified due to the high stiffness (115.00 N/μm) of the actuator. The simplification results only in local (close to the excitation point) inaccuracies of simulation. The load was applied as a sine function modulated by the Hann window. Material parameters and geometry of the model as well as parameters of excitation load (number of cycles of sine, frequency) were introduced in ABAQUS based on experimental data. The connection between the rod and the concrete cover was concerned as rigid and modeled as tie constraint. In the case of modeling the debonding between mortar cover and steel rod, the connection between steel and concrete was not defined at a debonding length.

The main aim of the numerical study was the verification of the theoretical description of the wave propagation phenomenon, while the signal amplitude was not considered as an indicative parameter in the adhesive bonding state assessment. Therefore, the damping effects were neglected in simulations.

2.3 Wave excitation

The experimental tests were conducted for several various excitation frequencies but the results in the paper are presented for the frequency of 50 kHz. For this frequency, the signals were characterized by the high amplitude and readability (high signal to noise ratio), which significantly improved their interpretation. However, the theoretical reasoning presented in the further sections is valid also for other excitation frequencies. The excitation was in the form of ten-cycle sine function modulated by a Hann window:

$$p(t) = \begin{cases} p_0 \sin(2\pi f t) \cdot 0.5\left(1 - \cos\left(2\pi f t / n_w\right)\right), & t \in (0, T_w) \\ 0 & t \geq T_w \end{cases} \tag{3}$$

where n_w is the number of the counts in the tone burst and f is the excitation frequency. Guided waves were propagated and received with the use of the PAQ-16000D device. The signals were registered with the use of the compressive-type transducers Noliac NAC2012. The transducers were characterized by the free stroke of 3.3 μm and blocking force of 378 N. The piezo elements were made of ceramic, orthotropic material and use the piezoelectric effect. Through the multilayer structure (the ceramic thin layers are separated by the inner electrodes) a control signal with the nominal voltage to 150V results in high electric field strength and deformations (strain up to 1.65 per mill) in a direction perpendicular to the plane of the actuator. The photographs of the experimental set-up and the transducer attached to the concrete cover are given in Figure 3.

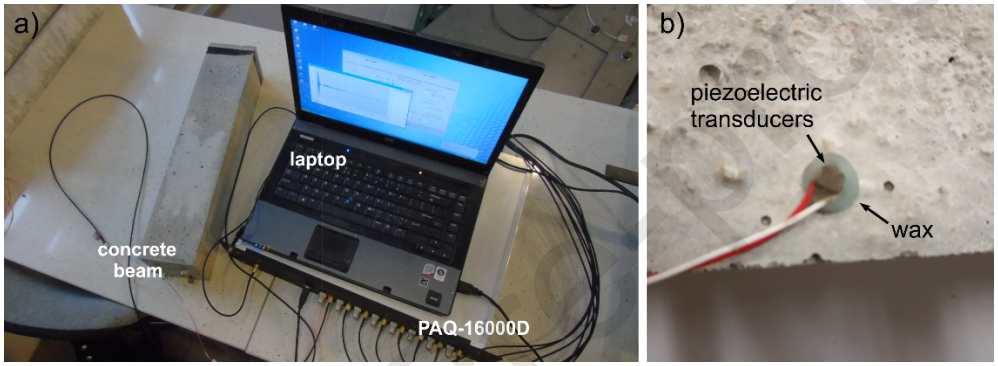

Figure 3 a) experimental set-up and b) transducer mounted on the concrete surface

2.4 Transducers configurations

The investigation was divided into three stages. Within each stage, the transducers were attached at the concrete surface and the wave excitation and signal registration were realized above of the different reinforcing rods (Figure 4). The experimental tests were conducted for five beams (Figure 2) for rods #1, #2 and #3. Because of cross-section symmetry about the diagonal, the results obtained for rod #4 are not discussed here.

During experimental tests, we had prior knowledge about the reinforcement location. In the cases of the real structures, the information about rebars location can be obtained using other nondestructive methods based on i.e. ground-penetrating radar or ferroscanning.

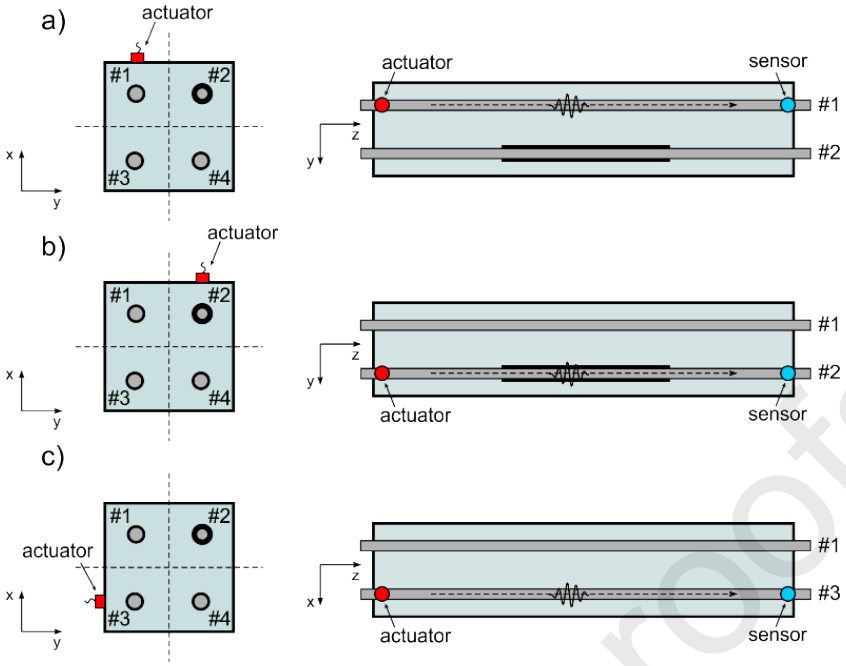

Figure 4 Transducers configurations: excitation and registration along the rod a) #1, b) #2 and c) #3

3. Theoretical description of flexural wave propagation in RC beam

Guided waves are dispersive waves, which means that their velocity and number of excited wave modes depend on the excitation frequency [40]. The relation between group velocity and the number of wave modes is usually illustrated by the dispersion curves. Their shape and the number depends on material parameters, as well as on the geometry of the cross-section. In some special cases (i.e. rod with circular cross-section) the dispersion curves can be determined by solving explicitly given dispersion equations. In the case of more complex cases like RC-beams, the dispersion equation cannot be given explicitly and the solution requires a different approach. Exemplary, Figure 5 presents the dispersion curves for two types of cross-sections considered in the paper. Black dots represent the dispersion solution for reinforced concrete RC cross-section with four perfectly bonded reinforcing bars. The solid line represents the dispersion curve determined for totally debonded reinforcing steel bar. The dispersion curve for the steel bar was obtained by solving the explicitly given dispersion equation presented in [41] using our code developed in the MATLAB environment. Because in this study the transducers were attached on the concrete surface and the excitation was perpendicular to the beam surface (Figure 4), dispersion curves only for flexural wave modes were taken into account and there was no need to consider the dispersion equations for other modes families (longitudinal and torsional). The dispersion curves for more complex RC cross-section were plotted with the use of free software GUIGUW (Graphical User Interface for guided Ultrasonic Waves) based on the semi-analytical finite element method [42]. The employed software does not allow to distinguish the selected curves, so the family mode can be recognized only based on the associated wave mode structures. Several wave modes with the highest velocity for a particular frequency have been recognized and appropriately signed in the figure (longitudinal - *L*, flexural - *F*, torsional - *T*).

The complexity of the dispersion solution strongly depends on the geometry and the material parameters of the cross-section. It can be seen that for a single steel bar only one dispersion curve was plotted, while in the case of RC cross-section, the number of possible solutions of the dispersion equation is significantly larger. The excitation of any frequency entails multimode propagation, which generally hinders the interpretation of the results.

Because the shape of dispersion curves for RC cross-section and separated rod and in consequence wave velocities differ, monitoring the velocity can be efficiently used in debonding detection, which is the main assumption of the developed approach. Due to the debonding development, the cross-section changes, and in consequence, the shape of the dispersion curves and wave velocity also changes. The knowledge about the dispersion solution is an important prerequisite in the analysis of wave velocity changes due to damage occurrence. In this section, we present the theoretical derivations about the influence of debonding length on wave propagation velocity based on dispersion curves. Two different scenarios varying in transducers placement were considered and described. First, the case of wave excitation and registration above the debonded bar was considered. Next, the description of the wave propagation phenomenon after excitation and registration above the bonded bar was presented. The

differences between these scenarios are the basis of the developed baseline-free damage detection method.

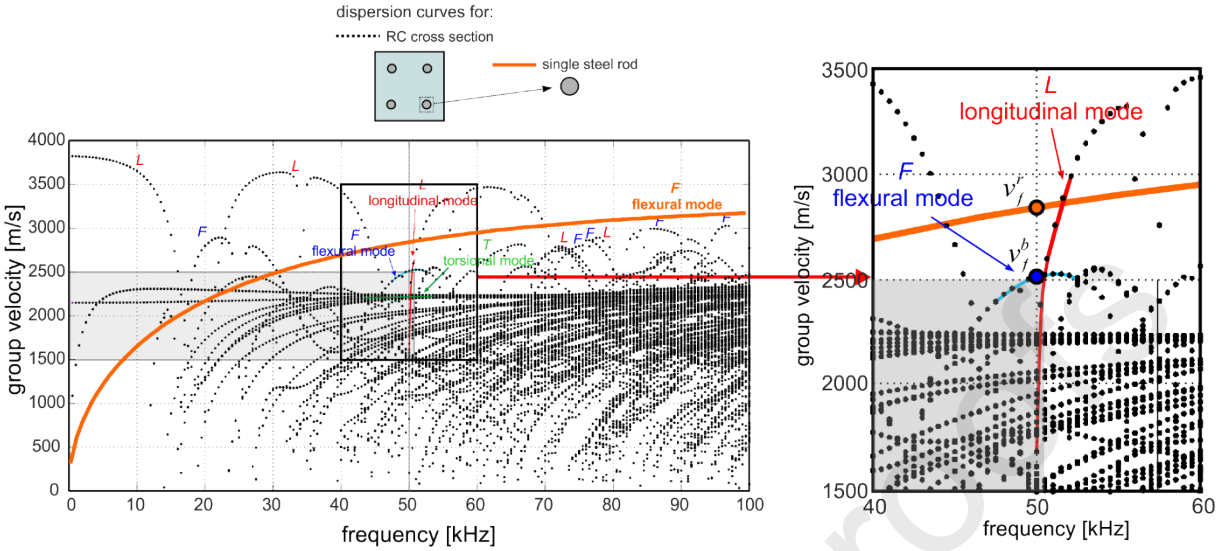

Figure 5 Dispersion curves plotted for reinforced cross-section (●) and for reinforcing rod (solid line)

3.1 Excitation above the debonded bar

In the first step, let's consider the case of a beam with an actuator and sensor placed exactly above the debonded bar (Figure 6a). The length of the specimen is L, while the debonding length is L_D. Perpendicular wave excitation entails the propagation of flexural wave mode. Its velocity v_f^b can be determined based on the dispersion solution. In the frequency range of 0-100 kHz, only one flexural wave mode can be excited in the single steel rod and therefore the velocity determination is not problematic (see Figure 5). However, in the case of the RC beam, the number of possibly excited wave modes is significantly higher. If several wave modes are excited, the velocity of the fastest wave mode must be taken into consideration because it is registered in the signal first. Thus, in the further considerations, we will take into account only the fastest wave mode excited for the particular frequency.

Excited wave travels along the undamaged length of the bar and diffracts at the start of debonding (Figure 6b). In the place of damage occurrence, the mode conversion phenomenon takes place. The diffraction causes that part of wave energy travels in concrete casting, while part travels along the separated waveguide. The velocities of waves propagating in separated beam parts are different, but usually, the velocity of the wave propagating in the steel rod is higher. The flexural wave mode propagating in the RC beam is converted info flexural wave mode propagating in the steel rod. The flexural mode triggered in steel bar propagating with velocity v_f^r (see Figure 5) again diffracts at the end of debonding. Along the bonded length wave again travels with a velocity equal to the velocity of the fastest mode in RC cross-section (Figure 6c).

The description of the phenomenon is supported by the results of the numerical investigation presented in the form of visualizations (Figure 7). The snapshots in selected time instants present the accelerations and deformations caused by wave motion in beam #C with debonding of 30 cm along the rod #2 (Figure 2). The visualization obtained numerically coincides well with the theoretical description presented in Figure 6.

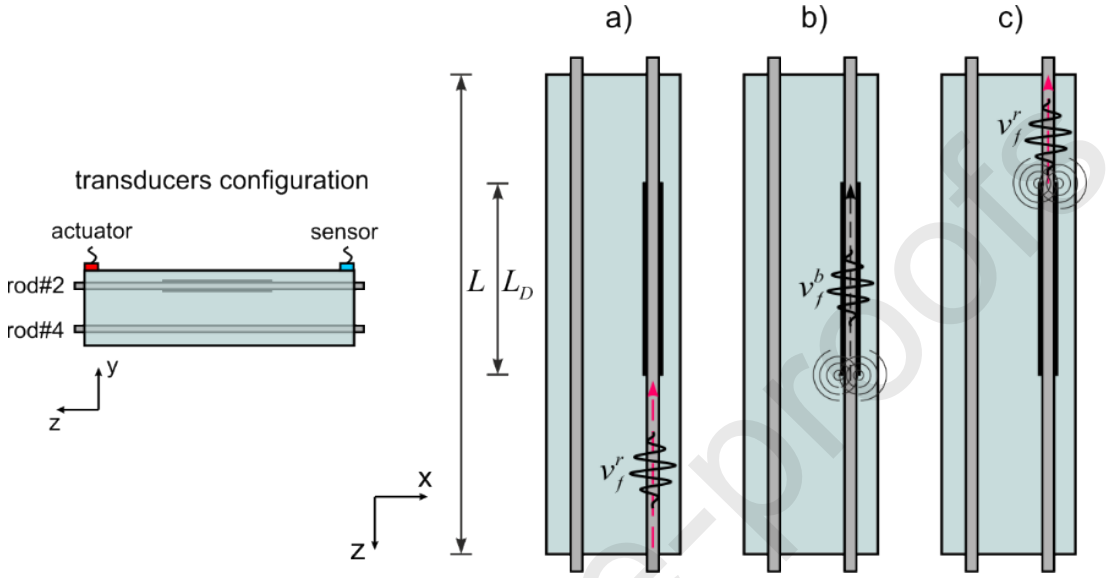

Figure 6 Wave propagation in concrete beam with debonding: a) wave excitation, b) diffraction at the start of debonding and propagation along the separated rod and c) diffraction at the end of debonding and propagation along the bonded bar

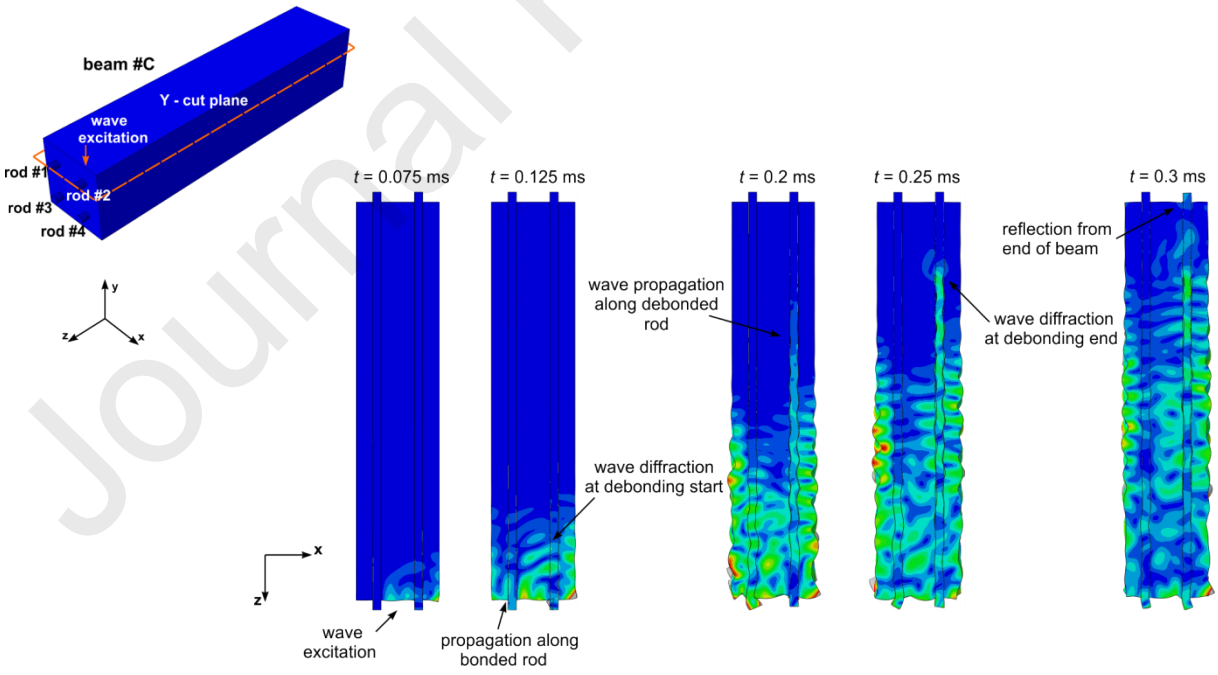

Figure 7 Numerical visualization of wave propagation in concrete beam with debonding damage after excitation above the debonded rod

Based on the description of the phenomenon we can derive the relationship between ToF of the first arriving wave and damage length:

$$t_D = \frac{L - L_D}{v_f^b} + \frac{L_D}{v_f^r} = \frac{L v_f^r - L_D\left(v_f^r - v_f^b\right)}{v_f^r v_f^b} \tag{4}$$

and the flexural wave velocity and damage length:

$$v_D = \frac{L v_f^r v_f^b}{L v_f^r - L_D\left(v_f^r - v_f^b\right)} \tag{5}$$

According to Eq. (3) if $v_f^r > v_f^b$ the increase of L_D will cause a decrease in the ToF.

3.2 Excitation above the bonded bar

If the excitation is performed above the bonded rod, the description of the phenomenon is more complex. Two scenarios may be distinguished. In the first scenario, the wave propagates along the fully bonded bar (Figure 8a). The ToF can be easily calculated as:

$$t_B^I = \frac{L}{v_f^b} \tag{6}$$

The first scenario takes place if the adjacent bars are fully bonded or the debonding is characterized by an insignificant size. Exemplary, the numerical simulations performed for undamaged beam #A illustrate this case (Figure 9). After wave excitation (t = 0.075 ms) above the rod #2 wave energy is immediately transferred into concrete cover and neighboring reinforcement. Flexural wave propagates in the entire volume of the specimen. The continuity of displacement and acceleration fields at the border of media is clearly visible at each time step.

The scheme of the second scenario is presented in Figure 8b. The theoretical description is supported by numerical results obtained for beam #C presented in Figure 10. In the second scenario after the excitation wave spreads and reaches the debonding damage located along the adjacent bar (Figure 10, t = 0.2 ms). If we assume that along the lengths L_B^1 and L_B^2 wave travels with velocity v_f^b, the total ToF can be calculated as:

$$t_B^{II} = \frac{\frac{L_B^1}{\sin\alpha} + \frac{L_B^2}{\sin\beta}}{v_f^b} + \frac{L_D}{v_f^r} = \frac{L_B^1 v_f^r\left(\sin\beta - \sin\alpha\right) + L_D \sin\alpha\left(v_f^r + v_f^b \sin\beta\right)}{v_f^b v_f^r \sin\alpha \sin\beta} \tag{7}$$

In the second case, the wave path is longer, however, the wave usually travels faster along the debonded bar. Therefore, it is difficult to predict the exact ToF of the first reflection registered in the signal. The general expression can be written as:

$$t_B = \min \begin{cases} t_B^I \\ t_B^{II} \end{cases} \tag{8}$$

The ToF of the incident wave excited above the fully bonded bar can be described by Eq. (5) or Eq. (7) depending on the values of the wave mode velocities and the debonding length. Regardless, which expression (Eq. (6) or Eq. (8)) describes the ToF after excitation above the bonded rod, if the velocity of flexural wave mode in a separated rod is higher than the velocity of flexural mode in RC beam $v_f^r > v_f^b$ the ToF is shorter if the excitation is realized above the debonded bar ($t_D < t_B$). Therefore, the registration of the different velocities in different parts of the beam may indicate the damage occurrence, which is used in the novel procedure of debonding detection.

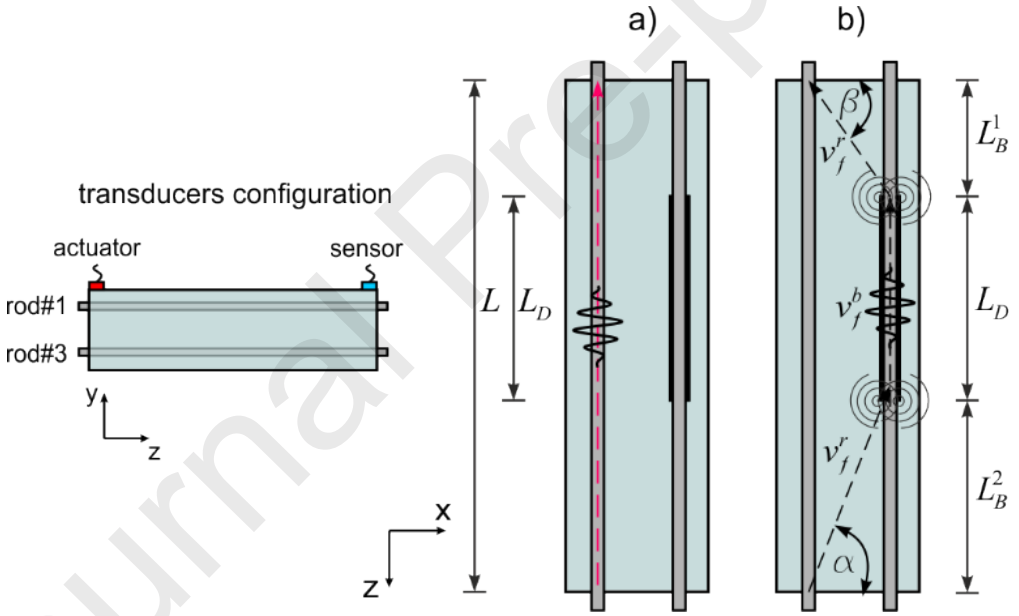

Figure 8 Wave propagation in concrete beam with debonding after excitation above the bonded rod: a) propagation along bonded rod and b) propagation along the debonded rod

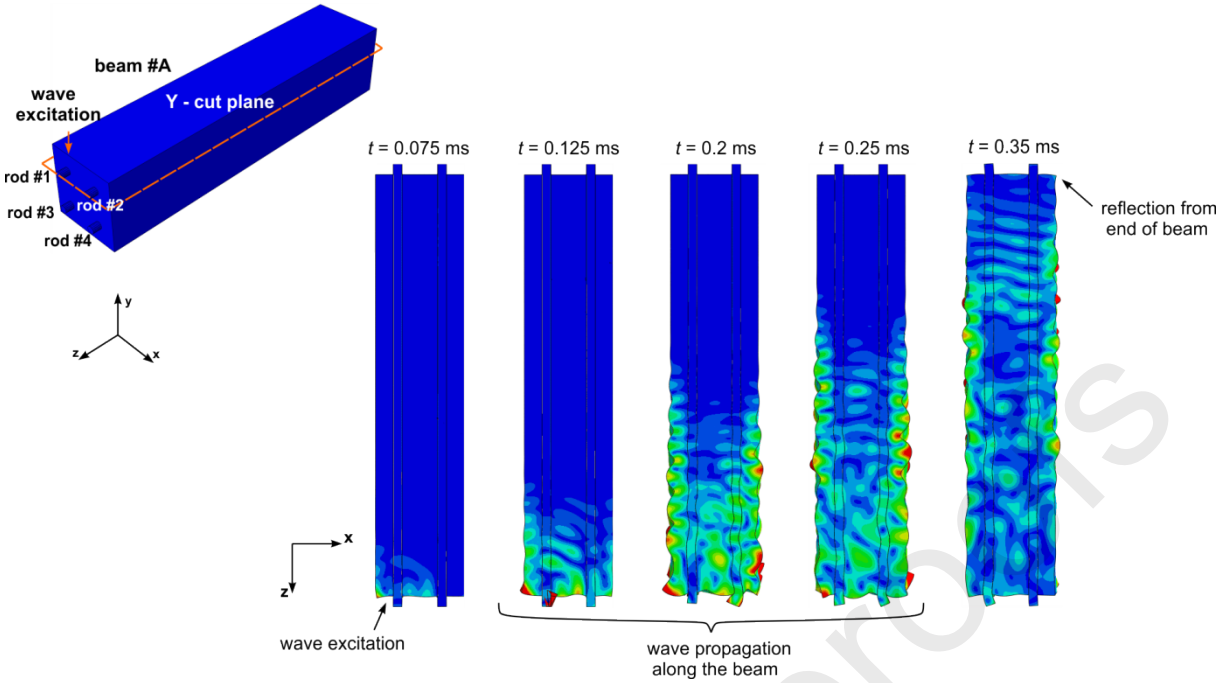

Figure 9 Numerical visualization of wave propagation in concrete beam #A after excitation above the bonded rod #1

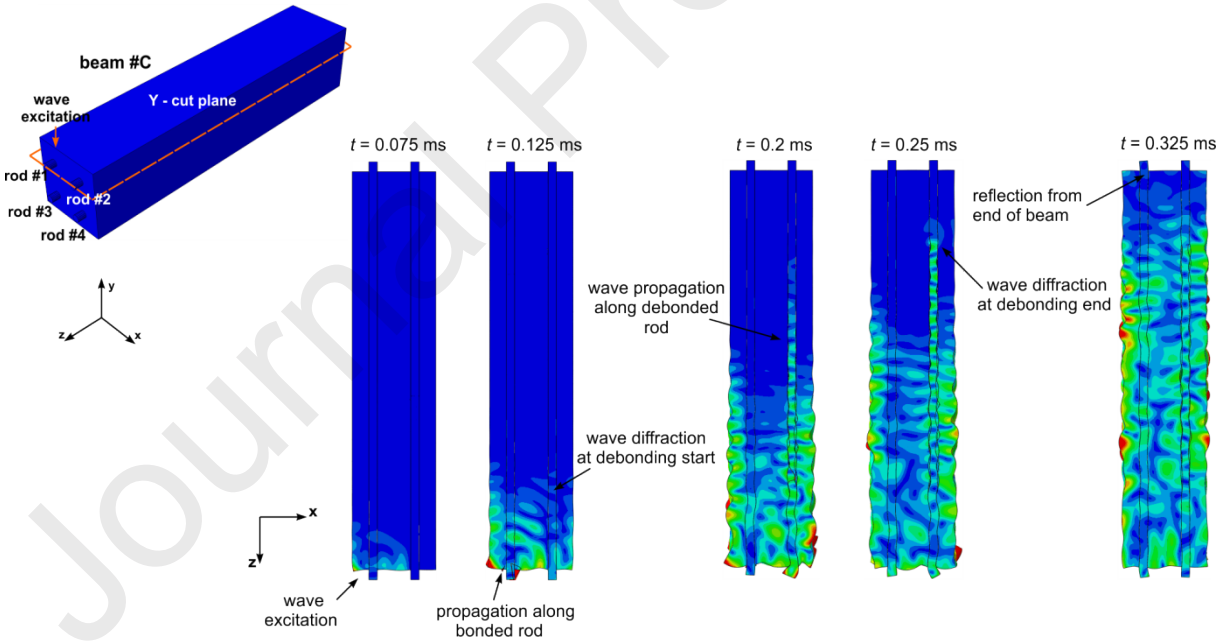

Figure 10 Numerical visualization of wave propagation in concrete beam #C with debonding damage after excitation above the bonded rod #1

4. Results of the experimental investigation

The experimental study was conducted to verify the correctness of the theoretical reasoning. It was divided into three main stages. In the first stage, the debonded rod is identified. Next, the theoretically and experimentally results are compared. In the last stage, the attempt of the exact damage length determination is made.

4.1 Stage I - identification of the debonded rod

In the first step, the theoretical and experimental velocities in the RC beam and steel rod were determined. For the considered excitation frequency of 50 kHz the theoretical velocities $v_f^{b,t}$ and $v_f^{r,t}$ determined based on dispersion curves are equal to 2512.5 and 2839.84 m/s, respectively (Figure 5). Because the theoretical considerations concerned the ToF of the first arriving wave packet, the velocity $v_f^{b,t}$ was determined for the fastest flexural wave mode.

To determine the experimental velocities in the RC beam and free steel waveguide, three piezo elements were attached at the surface of the specimens. Because the distance between the transducers was known, the velocity was easily calculated based on the ToFs obtained for signals registered by particular sensors (Figure 11). The ToF was determined using the conventional approach, which assumes that the ToF is the difference between registration times of two peaks greater than the threshold ([43],[44]). In general, if the signal to noise (SNR) ratio is low and the noise amplitude is comparable to the waveform amplitude, the reflections are difficult to extract and the estimated ToF value may be burdened with significant inaccuracy. The noise level, and thus the threshold value, depends on several various factors like the level of excitation, response, and noise floor of the instrumentation. Establishing the threshold requires the knowledge about the standard deviation of the noise level because the threshold level τ is usually defined to be *m* times the standard deviation of the noise. In the presented case, the amplitudes were relatively high because of the short propagation path. Moreover, as mentioned in section 2.3, before experimental tests, we have performed the sensitivity analysis to choose the excitation frequency providing a high SNR ratio. Additionally, the noise level was reduced by averaging multiple measurements. Thus, to avoid the overestimation of the ToF, the parameter *m* was relatively low and was equal to 3.

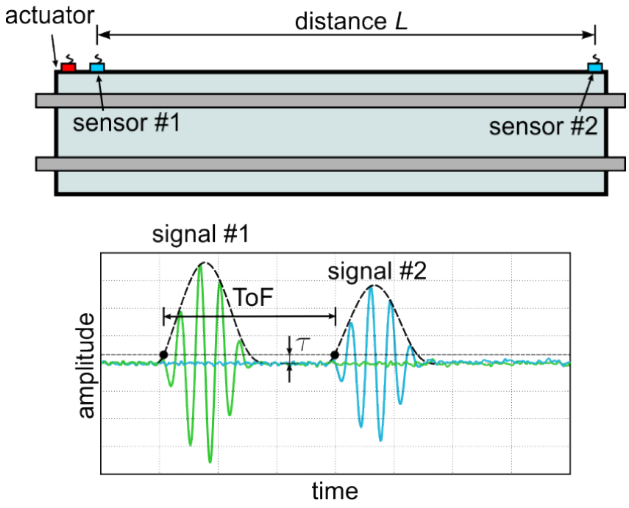

Figure 11 Determination of the ToF based on time-domain signals

The average experimental velocity in the RC beam was $v_f^{b,e} = 2301$ m/s and in steel waveguide $v_f^{r,e} = 3199.8$ m/s. The theoretical and experimental results are different, which may be caused by several factors. First of all, the geometry of experimental models is usually imperfect, while the theoretical calculations were made for perfect, symmetric cross-sections. Secondly, the dispersion curves were plotted for homogeneous, isotropic materials, while the concrete is strongly heterogeneous material. The influence of complex concrete mesostructure on wave velocity has been presented in several recent papers [35]-[39]. It was proved that not only the averaged material parameters influence the dispersion solution, but also the amount and size of aggregate particles. Moreover, the material parameters determined during destructive tests may slightly differ from the material parameters of the investigated specimens. The next reason for the velocity discrepancies is possible mode conversion resulting in excitation of the longitudinal modes. Even though the excitation was perpendicular and should result only in the excitation of the flexural modes, the imperfect transducers attachment or imperfect geometry could result in triggering also longitudinal wave modes. Please notice, that in the case of the longitudinal mode in the RC beam the dispersion curve is characterized by a relatively large slope (see Figure 5), which means that its propagation is related to a strong dispersion effect: different frequencies travel with different velocities, which leads to spreading the wave packet. Because it is usually difficult to maintain the mode purity, the theoretical dispersion curves can be treated only as an approximation of the exact, actual velocity. Moreover, the velocity determination is affected by the parameter *m* adopted to calculate the threshold level (see Figure 11). High *m* value eliminates the noise influence on the wave packet shape but may lead to overestimation of the ToF. As mentioned, the experiments were conducted in favorable conditions so the *m* value was relatively low. On the other hand, the propagation paths were short, which hindered significantly the correct velocity estimation.

In the next step, the actuator and sensor were attached on the concrete surface above the reinforcing rods at the distance of 47.6 cm and the time-domain signals were registered. The exemplary signals registered for bonded rod#1 and debonded rod #2 are presented in Figure 12. The schemes of the actuator and sensor configurations are additionally presented at the top of the figure. As we can see, the amplitudes of the signals differ considerably. The sensor and actuator were attached with the use of wax (Figure 3b). In general, the amplitude of the signals depends on the state of the investigated specimen, the length of the propagation path and concrete aggregates distribution, but also on the quality of the transducers attachment, amount of wax, and its temperature. For this reason, the signal amplitude is not considered here as an indicative parameter in the steel-concrete bonding quality assessment. The signals registered during experimental tests are presented in different scales for the readability.

The incident waves were identified and distinguished with the grey color. Next, the ToF of the incident wave for each rod was calculated and summarized in Figure 13. As mention in Section 4.1, the ToF corresponded to the starting point of the incident wave packet (see Figure 11). The ToF was additionally reduced by the device delay.

It can be seen that the ToFs differed for various rods embedded in the same beam (Figure 13), which means that one can expect the debonding occurrence. Since debonding development was expected to increase the wave velocity, in each case the lowest value of the ToF was indicated with the red color. As expected, in three cases (beam #B, #C, and #D) the shortest ToF was registered for debonded rod #2. However, the results for the beam with the totally debonded bar completely disagree with theoretical predictions (Figure 13e), because for the debonded rod #2 the longest ToF was obtained. This discrepancy is explained in the further part of the paper.

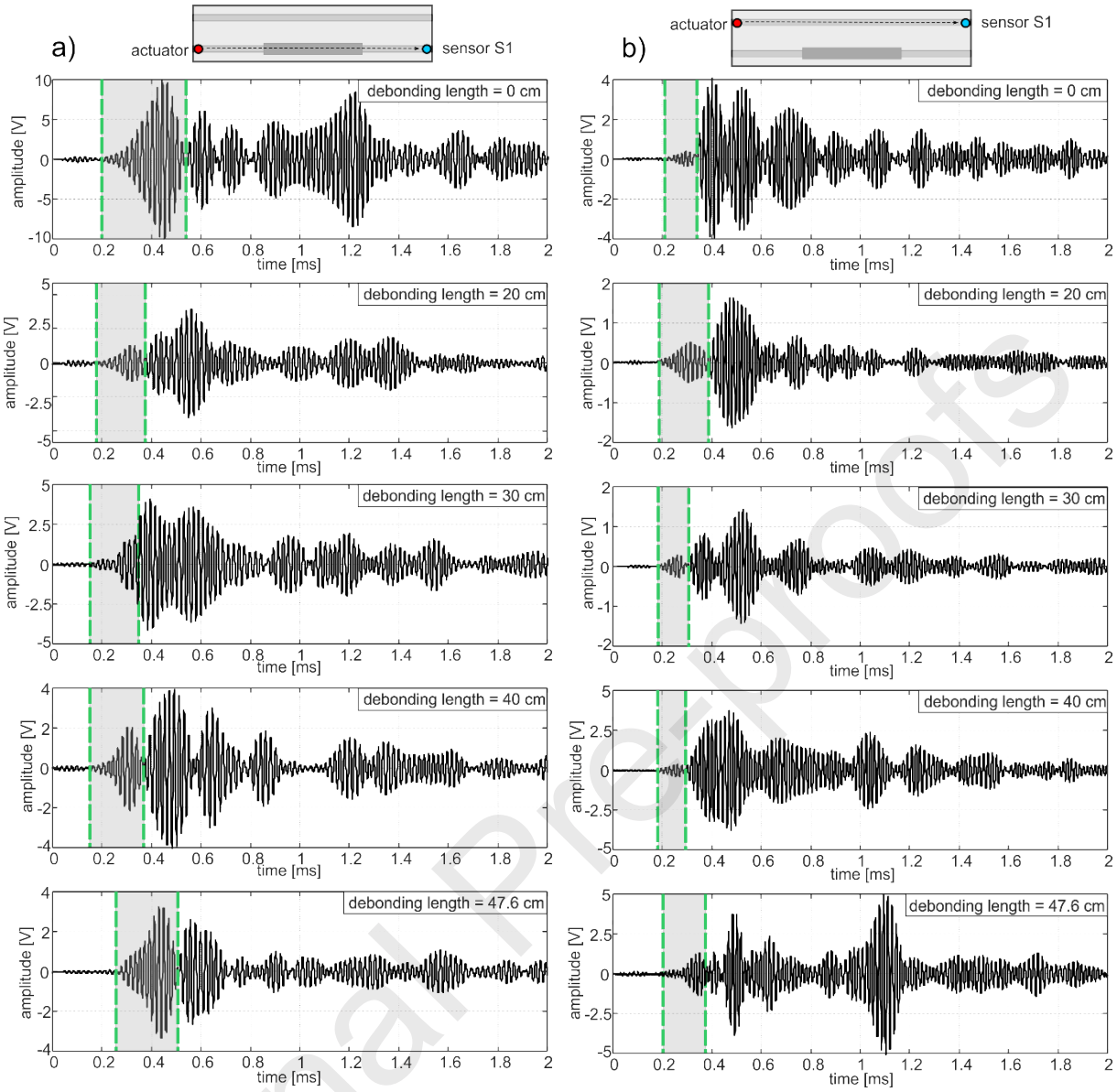

Figure 12 Experimental wave propagation signals registered a) along debonded rod and b) along bonded rod

To uniquely identify the location of the debonded rod, in the first step the maximum value of the ToF for the particular beam was indicated. As derived in Section 3, if $v_f^r > v_f^b$ the high quality of adhesive steel-concrete connection would result in lower velocity. Identifying the bar for which the ToF is the longest, allows to assess with what velocity the wave should propagate if the rod is fully bonded. In the next step, to compare the velocities registered within the same concrete beam, the ratios between the ToF obtained for rod i (i = 1,2,3) ToF_i and the highest value of the ToF_{max} obtained for the considered beam were calculated (Table 2). It can be seen that the disproportion between the ToFs for particular rods increases with increasing damage size. In the presented study we had a priori knowledge about the debonding length and location. For an unknown case, one would require a threshold that aided the qualification whether the rod is debonded or not. Based on the results obtained it was concluded that the

ratio threshold is equal to 0.95. If the shortest ToF is shorter than 95% of the longest ToF, the connection between steel and concrete is possibly damaged.

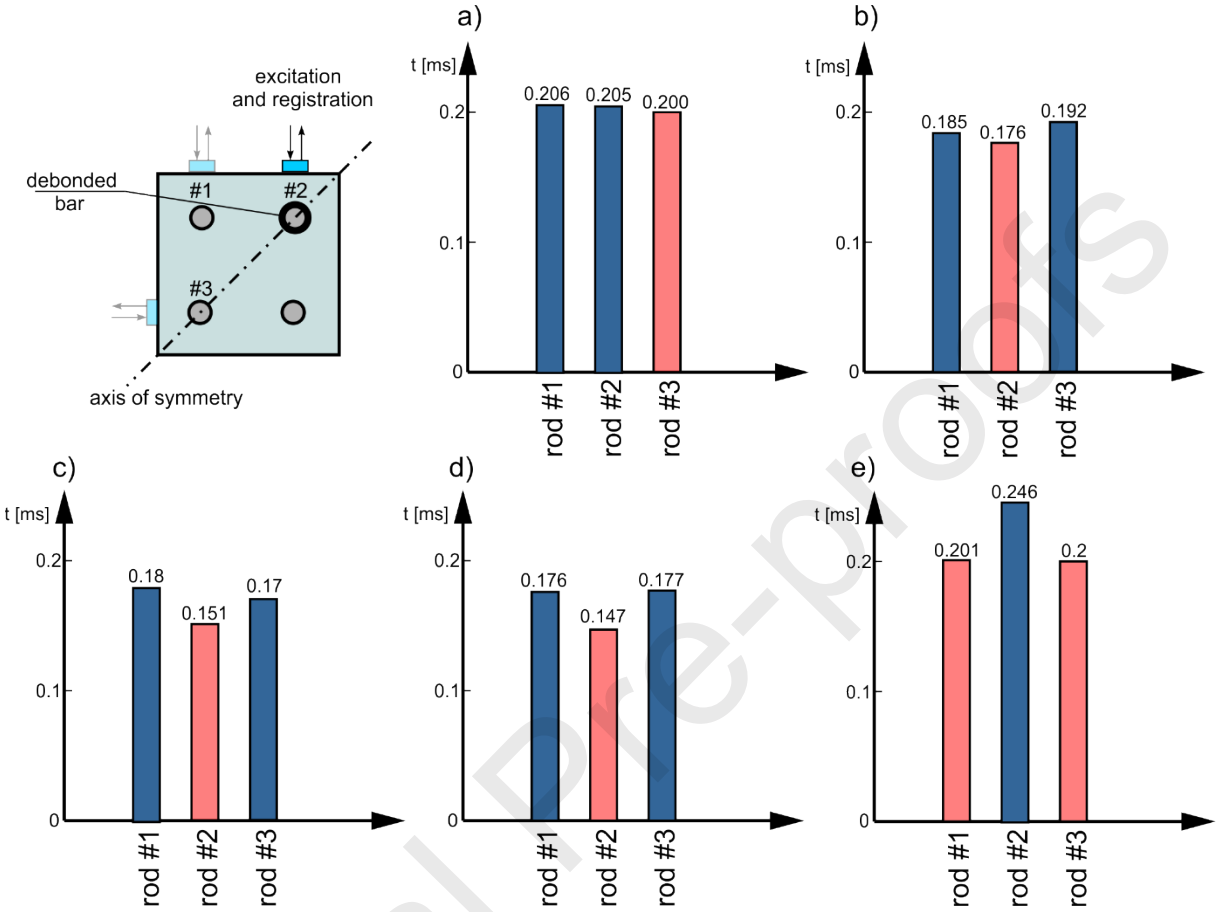

Figure 13 Experimental results in the form of the ToF registered for a wave propagating along reinforcing rods in beam a) #A, b) #B, c) #C, d) #D and e) #E

Following this recommendation, the values lower than 0.95 were marked in Table 2. The appropriate remarks concerning the state of the monitored object were made in Table 3. As we can see, in all cases the damaged beams (#B-#E) were identified correctly. Moreover, in three damaged beams, the lowest value of the ratio $\mathrm{ToF}_i / \mathrm{ToF}_{\max}$ was actually obtained for debonded rod #2, which means that the proposed method allows for both state assessment and debonded bar detection. Incorrect result was obtained only in the case of beam #E. The incompatibility of theoretical and experimental results for beam #E arises from the fact that the wave propagation phenomenon is completely different for fully debonded and partially debonded rods. The numerically obtained visualization of wave propagation in beam #E is presented in Figure 14. If the rod is totally separated, excited waves cannot be transferred into reinforcement and flexural wave modes traveling along the debonded rod with velocity v_f^r cannot be triggered. There are no changes in the beam cross-section, so we do not observe the diffractions at the start and end of the debonding damage. Wave velocity is constant and thus, the relationship (4) is

invalid for this case. The disproportion between the velocities for particular rods clearly indicates that damage occurs, but determining which rod is damaged is much more difficult in this case.

Table 2 ToFs for particular reinforcing rods in RC beams

	beam #A		beam #B		beam #C		beam #D		beam #E	
rod number	ToF	ratio ToF_i/ToF_{max}	ToF	ratio ToF_i/ToF_{max}	ToF	ratio ToF_i/ToF_{max}	ToF	ratio ToF_i/ToF_{max}	ToF	ratio ToF_i/ToF_{max}
#1	0.206	1.000	0.185	0.964	0.180	1.000	0.176	0.994	0.201	**0.817**
#2	0.205	0.995	0.176	**0.917**	0.151	**0.839**	0.147	**0.831**	0.246	1.000
#3	0.200	0.971	0.192	1.000	0.171	0.950	0.177	1.000	0.200	**0.813**

Table 3 Identification of the damaged specimens

beam	actual debonding length [cm]	Ratio ToF_{min} / ToF_{max}	remark
#A	0	0.971	undamaged beam
#B	20	0.917	possible damage occurrence
#C	30	0.839	possible damage occurrence
#D	40	0.831	possible damage occurrence
#E	47.6	0.813	possible damage occurrence

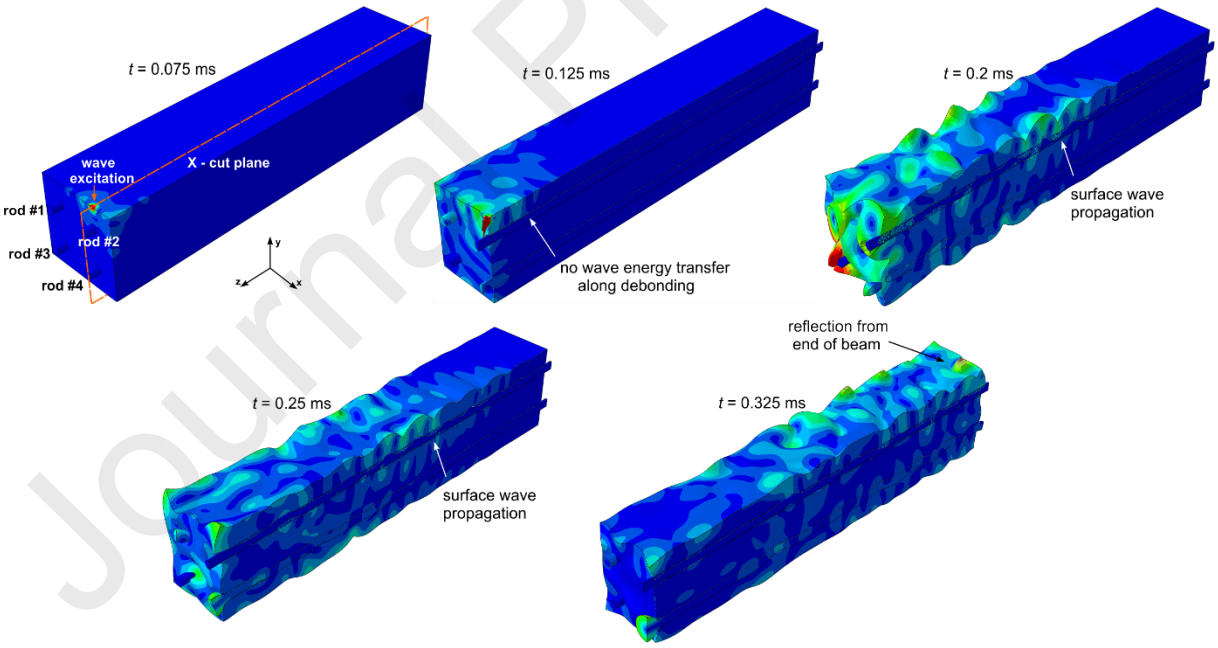

Figure 14 Wave propagation in RC beam with totally debonded steel rod after excitation above the debonded rod

The discrepancy between the results obtained for beam #E may be the results of the propagation of surface wave excited in the concrete casting above the debonded bar (Figure 14). The theoretical surface wave velocity can be calculated as:

$$c_R = \frac{0.87 + 1.12\nu}{1+\nu}\sqrt{\frac{\mu}{\rho}} \tag{9}$$

and μ is concrete shear modulus. The theoretically determined velocity is 2086.89 m/s and the ToF for the specimen of total length 0.476 m is 0.23 ms, which coincides well with the obtained result for fully debonded rod #2 (ToF = 0.246 ms, see Figure 13).

As we can see, this stage of the experiment indicated that the debonded rod detection is possible by using the velocities measured along different wave propagation paths in the same specimen. The main drawback and the direction of further research is the threshold estimation. We have assumed that the debonding damage occurred if the (CO JEST NIE TAK).

4.2 Stage II - comparison of experimental and theoretical data

After the identification of the debonded and bonded rods, the appropriate theoretical relationship describing the relation between ToF and debonding length and experimental results were compared. Figure 15 presents the results for the rods, for which the lowest ToF was registered and were considered as debonded. Three curves were plotted. The red, solid line represents the relationship described by Eq. (4) for wave velocities $v_f^{r,t}$ and $v_f^{b,t}$ determined theoretically based on dispersion curves. The blue, solid line represents the relationship described by Eq. (4) for experimentally determined velocities $v_f^{r,e}$ and $v_f^{b,e}$. The experimental results obtained for debonded rods in particular beams are marked with black dots. In Figure 15 the ToF measured for the beam #E was omitted. The experimental results were approximated by the linear function based using regression analysis and the least-squares method. The qualitative assessment of the linear approximation was made using the correlation coefficient R-squared, which was equal to 0.94. In all cases, a clear decreasing trend is observed. The slopes of the approximation curve plotted by the dashed line and theoretical blue curve traced for experimentally determined velocities are similar, which means that both experimental and theoretical analyses indicated the similar impact of debonding length on the flexural wave velocity. The agreement of the results confirms the correctness of the developed debonding length-wave velocity relationship.

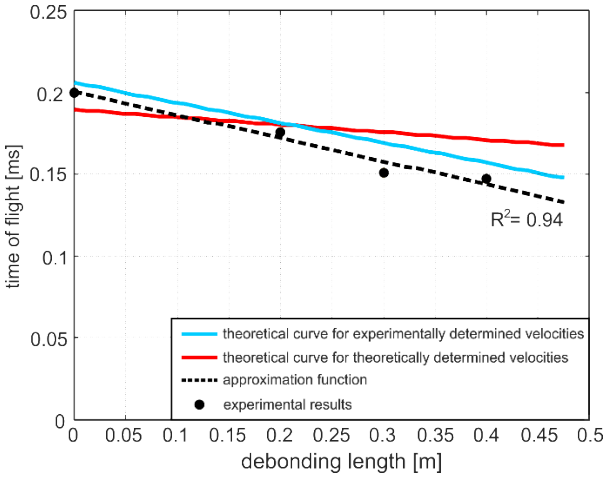

Figure 15 The comparison of theoretical and experimental relationship between the ToF measured above the bonded rod and debonding length

The results for the bonded rods are presented in Figure 16. As previously, the theoretical curve described by Eq. (8) was plotted for two data sets: theoretical (Figure 16a) and experimental (Figure 16b) flexural wave velocities. It can be seen that the relationship describing the ToF of the wave propagating in the bonded, adjacent rod is defined on intervals (see Eqs. (6)-(8)) and the shape of the curve differs significantly from the linear function derived for debonded rod (compare with Eq. (4)). The function has a global minimum, which means that both decreasing and increasing of debonding length may cause a wave velocity decreasing. The experimental results have confirmed the correctness of this relationship and showed that the ToF varies non-linearly if the excitation and registration is realized above the bonded rod. The theoretical curve determined for experimental wave velocities better reflects the actual shape of the experimental curves (Figure 16b). The compliance of experimental and theoretical results confirms that the adhesive steel-concrete connection is undamaged along the considered rods.

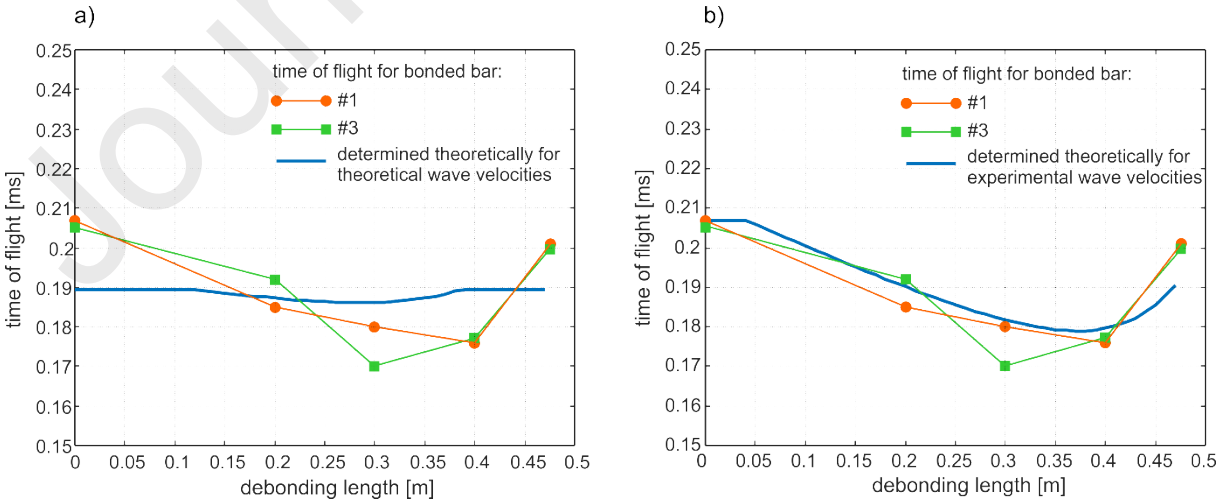

Figure 16 The comparison of theoretical and experimental relationship between the ToF measured above the debonded rod and debonding length

4.3 Stage III – the attempt of the debonding length determination

At the last stage of the investigation, after the identification of the debonded rods, the experimental results were used to determine the debonding lengths. Thus, the Eq. (4) was reformulated:

$$L_D = \frac{Lv_f^r - t_D v_f^r v_f^b}{v_f^r - v_f^b} \tag{10}$$

The results are summarized in Table 4. As previously, the debonding length was again calculated for two data sets: experimental and theoretical wave velocities. If the debonding length calculated was negative, which has no physical sense, it was assumed that L_D is equal to zero. The results presented allow to draw two important conclusions. First of all, the debonding length can be determined based on measured signals on the concrete cover, but the accuracy of the length estimation strongly depends on the accuracy of wave mode velocities determination. When the theoretical velocities established based on dispersion curves were used, the debonding length was overestimated. The overestimation results from the fact that the difference between theoretical velocities, which is the denominator in Eq. (10), is smaller than actual. The debonding length calculated for experimental velocities allows for a more accurate estimation of the debonding size. The insignificant differences between the outcomes may result from the inaccuracies in the ToF determining or non-perfect transducers placement.

The second conclusion concerns the beam #E with a totally debonded rod. The debonding was underestimated, which confirms that the propagation phenomenon differs for such an extreme case and the derived relationships are not valid here. The presence of damage was clearly indicated by a significant disproportion between the ToFs measured along particular rods (see Figure 13e), however, the exact location of debonded rod and debonding size cannot be determined in the same way as for beams with partial debonding.

Table 4 Determination of debonding length

beam	debonding length L_D [cm]	ToF [ms]	debonding length for theoretical velocities L_D^t [cm]	absolute error $\lvert L_D - L_D^t \rvert$ [cm]	debonding length for experimental velocities L_D^e [cm]	absolute error $\lvert L_D - L_D^e \rvert$ [cm]
#A	0	0.2	0.00	0	5.62	5.62
#B	20	0.176	28.23	8.23	24.88	4.88
#C	30	0.151	83.82	53.82	45.70	15.70
#D	40	0.147	92.54	52.54	49	9.00
#E	47.6	0.2	0	47.60	5	42.6

4.4 Discussion of aspects of practical applications

The presented approach allows for the detection of the debonded bar based on the differences in the ToF registered for various parts of the monitored specimen. The main advantage is no need of collecting any baseline data for an undamaged structure, which would be used in further comparative analysis. However, the practical application of the developed method must be preceded by the discussion of the disadvantages of the developed method.

In the article, the method of exact determining the debonding size was proposed. However, the proposed method is very sensitive for deviations in the ToF measurement, which is still a challenging task. A relatively small deviation in the ToF measurement may result in significant under- or overestimation of wave velocity, especially if the length of the propagation path is short. Moreover, the exact debonding size determination is possible only if the velocities in the debonded bar and undamaged beam are known. Two options are possible: experimental or theoretical determination of the velocities. The first option requires the reference data, which is from a practical point of view not always possible. The second option is related to the necessity of tracing and analysis of dispersion curves. The procedure of dispersion curves determination requires knowledge about the geometry of the cross-section and material parameters. Moreover, the complex mesostructure of the concrete specimens, as well as the presence of additional reinforcement may influences wave propagation phenomenon. Thus, the theoretical velocities may significantly differ from the actual ones. The recent papers proved that the dispersion curves determined for complex concrete specimens by solving the explicitly given dispersion equations differ from the dispersion curves obtained by particular models. Even if there is a possibility to trace the dispersion curves based on experimentally collected data, the wave velocities are approximate only. All these aspects cause that the baseline-free approach of debonding length determination based on theoretical velocities requires further development including the uncertainty analysis.

The possible solution, which would improve the efficiency of the presented method may be performing multiple measurements. In real cases, the reinforced concrete specimens are characterized by a significant size. The wave velocity can be measured in particular sections (Figure 17 – Stage I). The length of the inspection distance L depends directly on the energy of excitation. In the presented study the length of the propagation distance was equal to 50 cm, so we have used only one actuator-sensor pair. The propagation distance could be significantly extended by increasing the input voltage or by replacing the single transducer with the piezoelectric stack.

After the identification of the sections, where the velocity propagates with the significantly higher velocity, the configuration of the transducer is rearranged and the measurements are repeated in the sections, where possibly the debonding has developed (Figure 17 – Stage II). Moreover, the measurement can be made using various excitation frequencies. The developed method of debonded rod detection is more efficient if the difference between velocities of particular wave modes is significant. It is worth mentioning that the multiple measurements approach eliminates the problem of selecting the

method of the ToF calculation. The uncertainty in ToF measurement resulting from i.e. adopted threshold based on SNR is the same for all sections.

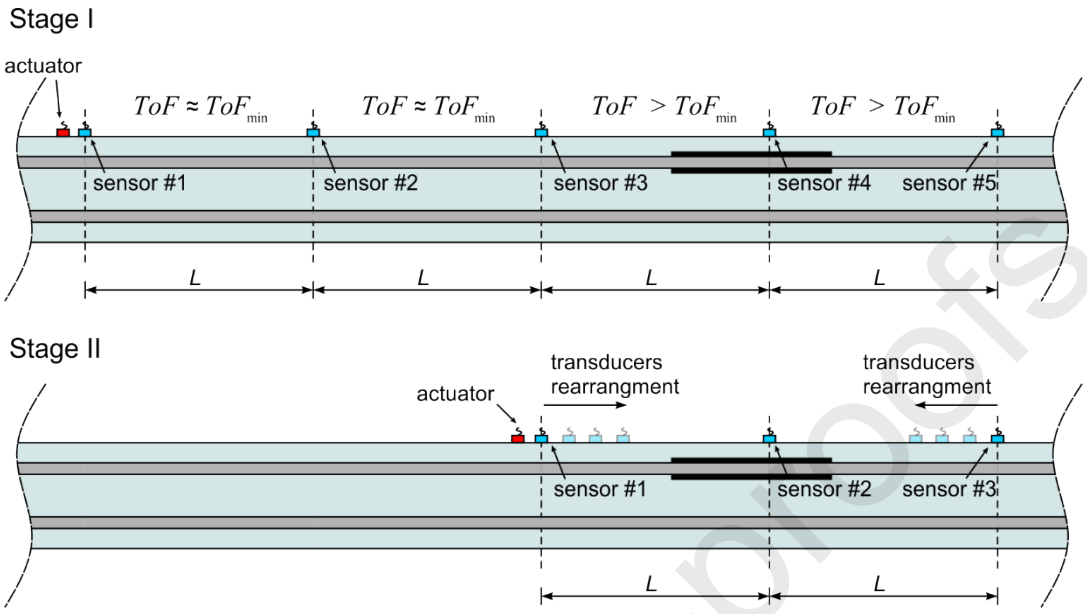

Figure 17 The procedures of debonding determination in large-size RC structures

Although the multiple measurements seem to be a potentially good solution in the case of real objects, it must be taken into account that the debonding occurrence influences the ToF but the proper interpretation of these changes can be more difficult in some cases. Let's consider the case of the beam with a debonded rod and the transducers attached along the bonded rod. As presented in section 3.2 the ToF of the excited wave may decrease, increase or remain the same depending on the debonding length. The relation between the ToF and the damage size depends on the bonded and debonded lengths, the position of the damage, and the wave mode velocities, which in turn depends on excitation frequency. Meanwhile, the relations between velocities and the excitation frequency are strongly nonlinear and cannot be given in an explicit form. All these aspects may result in fact that the investigator cannot be sure that the interpretation of the ToF differences is correct. Such uncertainties may be limited or reduced by conducting the additional measurements for various lengths of the propagation paths however the approach based on the multiple measurements is also not without flaws.

Below, the discussion of the effectiveness of the multiple measurements is presented. The analysis of concerns the variability of the ToF dependence on two different parameters: the debonding length and the distance between the transducers *d*. In the first step, it is assumed that the distance between the transducers *d* is changeable. In Figure 18 the relationship between ToF calculated acc. Eq. (7), distance *d* and debonding length L_D is presented in 3D graph. The calculations were performed for the experimental velocities $v_f^{b,e}$ and $v_f^{r,e}$ m/s. (see section 4.1). Additionally, the graph presented in Figure

18b presents the difference between the ToF obtained for damaged and undamaged beam calculated in the following way:

$$\Delta ToF = t_B - t_B^I \tag{11}$$

Based on these results, one can conclude that for each set of parameters (velocities $v_f^{b,e}$, $v_f^{r,e}$ and distance d) there exists a certain limit length of damage, which can be detected. Above this length, the modification of the mutual configuration of transducers without changing the distance d, will not affect the propagation velocity and the debonding remains undetectable. To minimize the risk of improper interpretation of the ToF changes, the measurements may be repeated for various distance d to check whether the variability of the ToF is consistent with theoretical predictions presented in Figure 18.

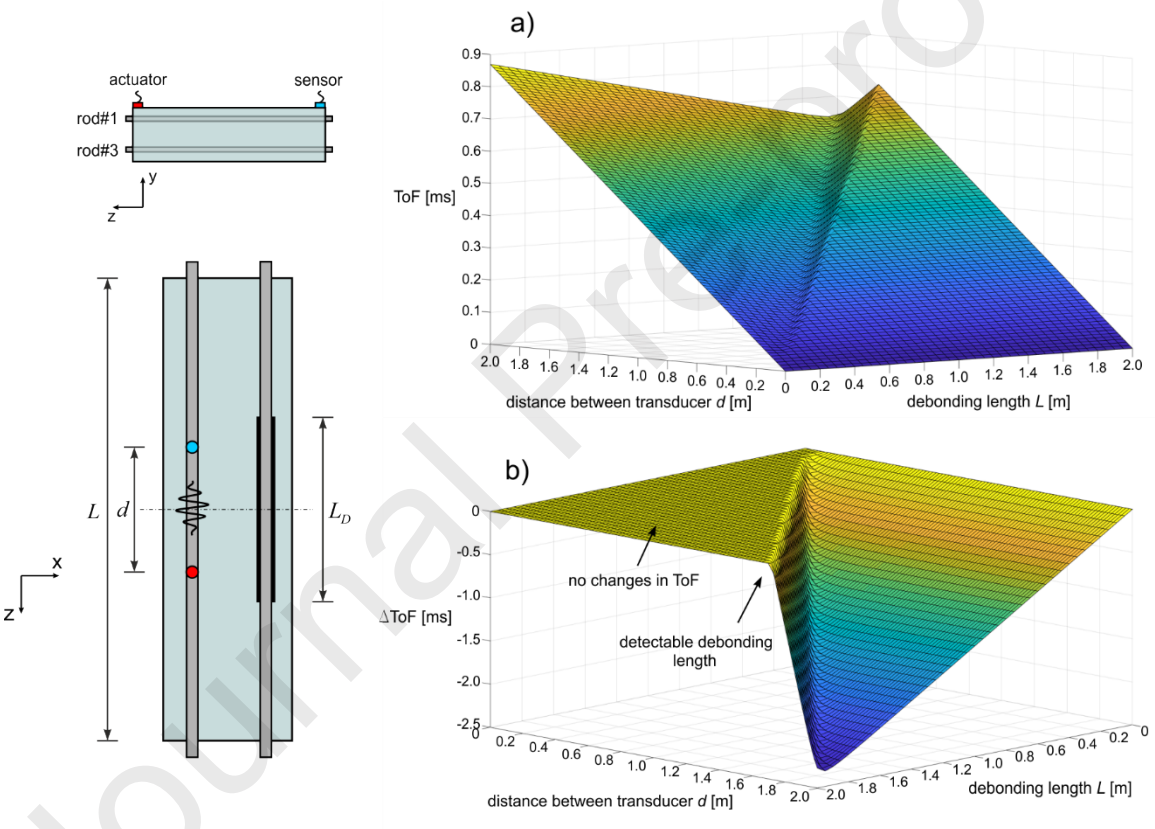

Figure 18 Values of the a) ToF and b) ΔToF calculated for damaged beam after wave excitation and registration above bonded rod

The next important issue requiring consideration is the adopted threshold of the ratio $\mathrm{ToF}_i / \mathrm{ToF}_{\max}$ which indicates the possible damage of the adhesive connection. In this study, the threshold was equal to 0.95, which is a high value indicating the considerable sensitivity of guided waves to debonding damage. The results obtained for damaged beams #B-#E were compared with results obtained for undamaged beam #A, which also allowed for adopting the relatively high threshold. But in fact, the

threshold value can be modified depending on the considered problem. In the case of specimens characterized by the more complex geometry or for shorter propagation distances, it is recommended to adopt a lower, less rigorous threshold value. Moreover, the threshold value should be established based on the difference in velocities v_f^r and v_f^b. In the case of a significant difference in velocities, even small damage would result in considerable velocity changes – thus, the threshold value can be lower than 0.95. If the velocities are comparable and the damage occurrence does not affect the average velocity, the threshold value should be higher to avoid the situation, when the dangerous damage remains undetected. Therefore, setting the threshold should be preceded by further research including the uncertainty analysis. Nevertheless, the developed method has the potential to be used in constant monitoring systems.

The last aspect, which must be considered in further studies, is wave interaction with other damage types. One of the assumptions of the wave propagation model in multilayered specimens describing dispersion relations is the continuity of displacement and stresses at the border of the layers. The discontinuities between layers disrupt the wave propagation phenomenon and influence propagation velocity. However, other forms of damages, such as concrete cracking, rebar corrosion, which take place at the same time, can hinder the interpretation of the results. Despite that, the localized damage like crack or corrosion pits usually result in additional reflections registered in signals, they can also influence wave propagation velocity and decrease the debonding size estimation accuracy. Changes in the wave propagation velocity always indicate the damage development, which can be used in diagnostics of other types of structural elements, however, unambiguous determination of its size may require the use of additional non-destructive diagnostic techniques.

5. Discussion and conclusions

The paper presents the results of numerical and experimental investigation of flexural wave propagation in RC beams with damage in the form of debonding between the steel rod and concrete cover. The research was focused on the unsolved issues related to the practical application of the wave propagation method in damage detection. The description of wave propagation phenomenon in the damaged beam allowed us to derive the relationships between debonding size and the ToF. Their correctness was verified and confirmed during experimental tests. Based on the conducted investigation, some important conclusions can be drawn:

- Debonding can be efficiently detected with the use of transducers attached to the concrete cover without the need for removing the concrete coating. The debonding development causes changes in wave propagation velocity measured in different parts of the investigated specimen.
- The placement of the transducers has an indisputable influence on the results. The results presented in the literature conducted for excitation and registration at the steel reinforcement suggest that in general wave velocity increases with increasing damage size ([44],[46]). Meanwhile, it is impossible to predict unequivocally whether wave velocity would increase or decrease with damage development without the information where the actuator and sensors are placed.
- The debonding length can be determined based on the measured signals, however, it requires an accurate determination of the velocities of flexural wave modes. In this study, the theoretical velocities determined based on dispersion curves differ from actual velocities. Therefore, to accurately determine the debonding size it is recommended to use the velocities determined experimentally on the undamaged object.

References

[1] Giurgiutiu V. Structural Health Monitoring with Piezoelectric Wafer Active Sensors, Academic Press, 2008.

[2] Su, Z. et al, Guided Lamb waves for identification of damage in composite structures: a review, Journal of Sound and Vibration 295 (2006) 753-780.

[3] Raghavan, A., Cesnik, CES., Review of guided wave structural health monitoring, Shock vibration Digest, 39(2) (2007) 91-114.

[4] Mitra, M., Gopalakrishnan, S. Guided wave based structural health monitoring: a review, Smart Materials and Structures 25(5) (2016) 27.

[5] Feng Q., Kong Q., Song G. Damage detection of concrete piles subject to typical damage types based on stress wave measurement using embedded smart aggregates transducers, Measurement 88 (2016) 345–352.

[6] Feng Q., Kong Q., Huo L., Song G. Crack detection and leakage monitoring on reinforced concrete pipe, Smart Materials and Structures 24 (11) (2015) 115020.

[7] Xu B., Zhang T., Song G., Gu H. Active interface debonding detection of a concrete-filled steel tube with piezoelectric technologies using wavelet packet analysis, Mechanical Systems and Signal Processing 36 (1) (2013) 7–17.

[8] Park S., Ahmad S., Yun C.B., Roh Y. Multiple crack detection of concrete structures using impedance-based structural health monitoring techniques, Experimental Mechanics 46 (5) (2006) 609–618.

[9] Wang D., Zhu H. Monitoring of the strength gain of concrete using embedded PZT impedance transducer, Construction and Building Materials 25 (9) (2011) 3703–3708.

[10] Tsangouri E., Aggelis D. A review of acoustic emission as indicator of reinfomrcement effectiness in concrete and cementitious composites. Construction and Building Materials 224 (2019) 198-205.

[11] Zaki A, Chai H.K., Behnia A., Aggelis D., Tan J.Y., Ibrahim Z. Monitoring fracture of steel corroded reinforced concrete members under flexure by acoustic emission technique. Construction and Building Materials 136 (2017) 609-618.

[12] Goszczyńska B, Świt G, Trąmpczyński W, Krampikowska A, Tworzewska J, Tworzewski P. Experimental validation of concrete crack identification and location with acoustic emission method. Arch Civ Mech Eng. 2012;12(1):23–8.

[13] Ohno K, Ohtsu M. Crack classification in concrete based on acoustic emission. Constr Build Mater. 2010;24(12):2339–46.

[14] Mpalaskas AC, Matikas TE, Van Hemelrijck D, Papakitsos GS, Aggelis DG. Acoustic emission monitoring of granite under bend-ing and shear loading. Arch Civ Mech Eng. 2016;16(3):313–24

[15] Verstrynge E, Schueremans L, Van Gemert D, Wevers M. Moni-toring and predicting masonry's creep failure with the acoustic emission technique. NDT E Int. 2009;42(6):518–23.

[16] Ng C-T., Mohseni H., Lam H-F. Debonding detection in CFRP-retrofitted reinforced concrete structures using nonlinear Rayleigh wave. Mechanical Systems and Signal Processing 125 (2019) 245-256.

[17] Chen H., Xu B., Zhou T., Mo Y-L. Debonding detection for rectangular CFST using surface wave measurement: Test and multi-physical fields numerical simulation. Mechanical Systems and Signal Processing 117 (2019) 238-254.

[18] Xu B., Chen H., Mo Y-L., Chen X. Multi-physical field guided wave simulation for circular concrete-filled steel tubes coupled with piezoelectric patches considering debonding defects. International Journal of Solids and Structures 122-123 (2017) 25-32.

[19] Liu T., Li J., Cai X., Yan S. A time-frequency analysis algorithm for ultrasonic waves generating from a debonding defect by using empirical wavelet transform. Applied Acoustics 131 (2018) 16-27.

[20] Feng B., Riberio A.L., Ramos H.G. Interaction of Lamb waves with the edges of a delamination in CFRP composites and a reference-free localization method for delamination. Measurement 122 (2018) 424-431.

[21] Beard M.D., Lowe M.J.S., Cawley P. Ultrasonic guided waves for inspection of grouted tendons and bolts. Journal of Material and Civil Engineering 15(3) (2003).

[22] Na W.-B., Kundu T., Ehsani M.R. Lamb waves for detecting delamination between steel bars and concrete. Computer-Aided Civil and Infrastructure Engineering 18 (2003) 58–63.

[23] Sharma S., Mukherjee A.: Longitudinal guided waves for monitoring chloride corrosion in reinforcing bars in concrete, Structural Health Monitoring 9(4) (2010) 555-567.

[24] Li D.S., Ruan T., Yuan J.H. Inspection of reinforced interface delamination using ultrasonic guided wave non-destructive test technique. Science China Technological Sciences 55(10) (2012) 2893-2901.

[25] Wu F., Chang F.-K., Debond detection using embedded piezoelectric elements in reinforced concrete structures – part I: experiment. Structural Health Monitoring 5 (2006) 5-15.

[26] Song G., Gu H., Mo Y.L., Hsu T.T.C., Dhonde H. Concrete structural health monitoring using embedded piezoceramic transducers. Smart Materials and Structures 16 (2007) 959-968.

[27] Zima B., Kędra R. Reference-free determination of debonding length in reinforced concrete beams using guided wave propagation. Construction and Building Materials 207 (2019) 291-303.

[28] Li Y., Lu Y., Lee Y.F. Debonding detection in CFRP-reinforced steel structures using anti-symmetrical guided waves. Composite Structures 253 (2020) 112813.

[29] Ervin, B.L.; Bernhard, J.T.; Kuchma, D.A.; Reis, H. Estimation of corrosion damage to steel reinforced mortarusing frequency sweeps of guided mechanical waves.Sens. Smart Struct. Technol. Civ.2006,48.

[30] Zima B., Rucka M. Guided ultrasonic waves for detection of debonding in bars partially embedded in grout. Construction and Building Materials 168 (2018) 124-142.

[31] Zima B., Kędra R. Debonding size estimation in reinforced concrete beams using guided wave-based method. Sensors 20 (2020) 1-18.

[32] Zima B., Kędra R. Evaluation of the resistance of steel–concrete adhesive connection in reinforced concrete beams using guided wave propagation. Archives of Civil and Mechanical Engineering 20(1) (2020).

[33] Xu, B., Luan, L., Chen, H., Wang, J., Zheng, W. Experimental Study on Active Interface Debonding Detection for Rectangular Concrete-Filled Steel Tubes with Surface Wave Measurement. Sensors 19 (2019) 3248.

[34] Moser F., Jacobs L.J., Qu J. Modeling elastic wave propagation in waveguides with the finite element method, NDT&E International, 32(4), 225-234, 1999.

[35] Chen H., Xu B., Zhou T., Mo Y-L. Debonding detection for rectangular CFST using surface wave measurement: Test and multi-physical fields numerical simulation, Mechanical Systems and Signal Processing, 117 (2019) 238-254.

[36] Wang Y., Li X., Wang Q., Xu B., Deng J. Debonding damage detection of the CFRP-concrete interface based on piezoelectric ceramics by the wave-based method. Construction and Building Materials, 210 (2019) 514-524.

[37] Zima B., Kędra R. Numerical Study of Concrete Mesostructure Effect on Lamb Wave Propagation, Materials 13(11) (2020) 2570.

[38] Iliopoulos, S. N., Aggelis, D. G. and Polyzos, D., Wave dispersion in fresh and hardened concrete through the prism of gradient elasticity. International Journal of Solids and Structures, 78–79 (2016) 149-159.

[39] Iliopoulos S., Malm F., Grosse C., Aggelis D. Experimental investigation of wave dispersion in hardened concrete and reference liquid media. Smart Materials and Nondestructive Evaluation for Energy Systems, Proceeding of SPIE, Vol. 10171, 2017.

[40] Rose JL. Ultrasonic guided waves in solid media. Cambridge University Press, 2014.

[41] Pao, Y.H.; Mindlin, R.D. Dispersion of flexural waves in an elastic, circular cylinder. J. Appl. Mech.1960,27,513–520

[42] P. Bocchini, A. Marzani, E. Viola, Graphical user interface for guided acoustic waves, J. Comput. Civil Eng. 25 (3) (2011) 202–210.

[43] Barshan B. Fast processing techniques for accurate ultrasonic range measurements. Meas. Sci. technology 11 (2000) 45-50.

[44] Heijden F., Duin R.P.W., Ridder T., Tax D.M.J. Classification, Parameter Estimation and State Estimation. An Engineering Approach using MATLAB. John Wiley and Sons, 2004.

[45] Yu J.–D., Bae M.–H., Lee I.–M., Lee J.–S. Nongrouted ratio evaluation of rock bolts by reflection of guided ultrasonic waves. Journal of Geotechnical and Geoenvironmental Engineering 139(2) (2013) 298– 307.

[46] Cui Y, Zou D.H, Numerical simulation of attenuation and group velocity of guided ultrasonic wave in grouted rock bolts. Journal of Applied Geophysics, 59(4) (2006) 337–344.